Journal of Materials Chemistry

Cite this: *J. Mater. Chem.*, 2011, **21**, 5704

www.rsc.org/materials

PAPER

Direct growth of β-$FeSi_2$ nanowires with infrared emission, ferromagnetism at room temperature and high magnetoresistance *via* a spontaneous chemical reaction method†

Shih-Wei Hung,[a] Ping-Hung Yeh,[b] Li-Wei Chu,[a] Chii-Dong Chen,[c] Li-Jen Chou,[a] Yi-Jen Wu[a] and Lih-Juann Chen*[a]

Received 16th January 2011, Accepted 17th February 2011
DOI: 10.1039/c1jm10232j

Self-catalyzed β-$FeSi_2$ nanowires with a high aspect ratio have been synthesized by a spontaneous chemical vapor transport and reaction method. The as-synthesized single-crystalline β-$FeSi_2$ nanowires exhibit photoluminescence at a wavelength of 1.54 μm, which is suitable for Si-based optical communication, at room temperature. The conductivity of a single-stem β-$FeSi_2$ nanowire was found to increase with decreasing diameter. The room temperature ferromagnetism and high magnetoresistance performance of 6% at 200 K indicates that β-$FeSi_2$ nanowires are potentially applicable for spintronic nanodevices.

Introducton

One-dimensional Si-based nanostructures have attracted much attention for their potential applications in electronic and optoelectronic nanodevices, as well as for their intriguing physical properties that are different from those of bulk materials.[1–7] For the synthesis of 1-D nanowires, metal-catalyzed chemical vapor deposition (CVD) has proven to be one of the most successful growth methods.[8–11] However, metal contamination is often detrimental to their applications.[12] As a result, catalyst-free growth of 1-D nanowires by various methods has become an important concern.[13]

Silicon nanostructures have long been the material for advanced microelectronic technology, but they are poor emitters of light due to their indirect bandgap. To develop Si-based nanostructures with excellent light-emission behaviors, materials, such as Si–Ge nanostructures and erbium-doped silicon were found to be good candidates due to their emission wavelength of 1.5 μm, which was crucial for optical fiber communication. However, erbium-doped Si nanowires suffered from residual defects and contaminations during the fabrication process; Si–Ge nanostructures are unsatisfactory due to relatively low luminescence efficiency and a broad energy distribution.[14] Therefore, both erbium-doped Si or Si–Ge are unsuitable for practical optodevice applications. As a result, materials compatible with Si-based optoelectronics, as well as with excellent infrared emission properties, are highly desirable. Semiconducting β-$FeSi_2$ is considered for its established light-emitting property at near 1.5 μm.[15] The direct gap characteristics, which are correlated to the band-edge-related luminescence, are advantageous for telecommunication applications as photonic crystals with a high refractive index.[16,17]

Synthesis of high-quality β-$FeSi_2$ on Si is compatible with Si-based device processing. Investigations of room-temperature photoluminescence or electroluminescence obtained from β-$FeSi_2$ thin films have been reported extensively.[15,18–20] For the observation of photoluminescence from β-$FeSi_2$ thin films, various growth methods, such as, ion beam synthesis (IBS), reactive deposition epitaxy (RDE), chemical vapor deposition (CVD) and molecular beam epitaxy (MBE) were used. However, reports on the growth of 1-D β-$FeSi_2$ nanowires have been scarce and their physical characteristics need to be further investigated.[21,22]

Recently, use of the magnetic semiconducting silicide of $Fe_{1-x}Co_xSi$ as injectors for spintronics applications has been reported.[23] Magnetic semiconductors have received considerable attention due to their large anomalous Hall effect (AHE). The AHE is important since it can be applied to meter the magnetization of the mesoscopic structures that would appear in fully integrated spintronics devices.[24] β-$FeSi_2$ also exhibits special features of AHE.[25] In this paper we report the growth and structural characterization of the self-catalyzed β-$FeSi_2$ nanowires *via* a spontaneous chemical reaction method in one step. The as-fabricated single crystalline β-$FeSi_2$ nanowires showed room temperature ferromagnetism. In contrast, in the case of the β-$FeSi_2$ thin film, ferromagnetism was

[a]*Department of Materials Science and Engineering, National Tsing Hua University, Hsinchu, Taiwan, ROC. E-mail: ljchen@mx.nthu.edu.tw; Fax: +886-3-5718328; Tel: +886-3-5731166*
[b]*Department of Physics, Tamkang University, Tansui, Taiwan, 251, R. O. C*
[c]*Institute of Physics, Academia Sinica, Taipei, Taiwan, R. O. C*
† Electronic supplementary information (ESI) available: XRD, SEM, TEM characterizations, EDS, diffraction pattern, sample preparation and growth mechanism. See DOI: 10.1039/c1jm10232j

found only at temperatures below 100 K. A combination of infrared emission, room temperature ferromagnetism and high magnetoresistance was found. The favorable properties will be conducive to applications in optical and spintronic nanodevices.

Experimental

Iron silicide nanowires were synthesized in a horizontal hot wall three-zone furnace by a chemical vapor transport method. The quartz tube was evacuated to 1×10^{-2} torr with a mechanical pump. During the growth of the iron silicide nanowires, a constant gas flow of 150 SCCM (SCCM denotes cubic centimetre per minute at STP) carrier gas of 80% Ar + 20% H_2 was introduced. The Si substrates were cleaned with 3 wt%-buffered HF prior to placing in the furnace. $FeCl_3 \cdot 4H_2O$ powders were used as the precursors and silicon (001) as the substrates, placed in the upstream and downstream zones, respectively. The upstream zone was heated from room temperature to 600 °C and the other two downstream zones were heated to 800 °C in 30 min. When the furnace reached the set point, the $FeCl_3 \cdot 4H_2O$ precursors produced vapor-phase $FeCl_3$ or Fe_2Cl_6 that was carried by the gas flow to the center of the furnace. The reaction was held under these conditions for 60 min, and then the furnace was allowed to cool to room temperature slowly.

The morphology of the iron silicide nanowires was examined with a field-emission scanning electron microscope (FESEM) (JEOL JSM-6500F). The microstructures and chemical compositions of the iron silicide nanowires were characterized using a 200 kV transmission electron microscope (TEM) (JEOL JEM-2010) equipped with an energy dispersive spectrometer (EDS). The room-temperature photoluminescence spectrum was excited with a 405 nm laser and obtained with an InGaAs photodiode detector. For single semiconducting β-$FeSi_2$ nanowire photoluminescence measurements, the as-synthesized nanowires were first dipped in dilute HF (3 wt%) for 10 s to remove silicon oxide layers at the surfaces. The obtained β-$FeSi_2$ nanowires were dispersed on Si substrates and characterized with a micro-photoluminescence (micro-PL) system. For the near-infrared (NIR) PL spectra reported herein, the background signal from the Si substrates has been subtracted. For the electrical property measurements, a focused ion beam (FIB) system was used to deposit platinum layer as contacts at the edges of β-$FeSi_2$ nanowires dispersed on the SiO_2/Si substrates. The magnetic properties were characterized with a vibrating sample magnetometer (VSM) device. The nanodevices for magnetoresistance measurements were fabricated by the standard e-beam lithography (EBL) processes *via* a nano pattern generation system (NPGS). β-$FeSi_2$ nanowires were dispersed on SiO_2/Si substrates with electrodes of 50 nm Ti and 100 nm Au followed by EBL processes. Aluminum was evaporated as leads. Before making contacts to the nanowires, the samples were treated with 80 W oxygen plasma for 30 s to remove the organic contaminants at the surface of the nanowires. The measurement was carried out in a Lab-View controlled physical properties measurement system (PPMS).

Results and discusson

Fig. 1(a) is an SEM image showing the formation of free-standing nanowires with inner-diameters 40–60 nm and lengths

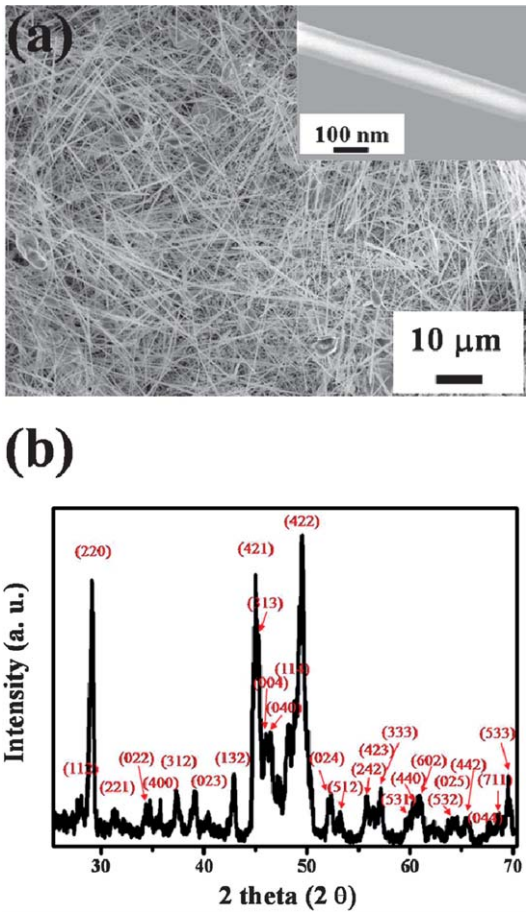

Fig. 1 (a) A SEM image of the free-standing β-$FeSi_2$ nanowires grown in the downstream zone. Inset: a higher magnification image and the core–shell structure can be observed. (b) GIXRD spectrum indicating that all diffraction peaks can be ascribed to the β-$FeSi_2$ phase with an orthorhombic structure.

30–60 μm. The aspect ratio of the β-$FeSi_2$ nanowire is more than 500. From the high-magnification SEM image, as shown in the inset, a core–shell structure can be observed. The core and shell are about 50 nm in diameter and 20 nm in thickness, respectively. Analysis of GIXRD spectra indicates that all diffraction peaks can be ascribed to the β-$FeSi_2$ phase with an orthorhombic structure, as shown in Fig. 1(b). During the formation of the β-$FeSi_2$ nanowires, stable silicon oxide shells would appear and wrap around the iron silicide cores. Shell layers play the role of retarding the rapid diffusion of Fe atoms into the iron silicide and preventing the lateral expansion of β-$FeSi_2$ nanowires, which results in high aspect ratio nanowires.

Fig. 2(a) shows the low-magnification TEM image of an individual β-$FeSi_2$ nanowire with a 33 nm core and 30 nm shell. Fig. 2(b) shows the EDS spectrum taken from the shell layer of the nanowire, which is composed of Si and O. No Fe or other impurities were found in this shell layer. Fig. 2(c) reveals the high-magnification TEM image of a β-$FeSi_2$ nanowire dipped in a dilute HF (3 wt%) solution for 10 s to remove the shell layer of silicon oxide. The EDS spectrum taken from the core layer shows that it is composed of Fe and Si with an atomic ratio close to 1 : 2, as shown in Fig. 2(d). Fig. 2(e) shows the SAED pattern

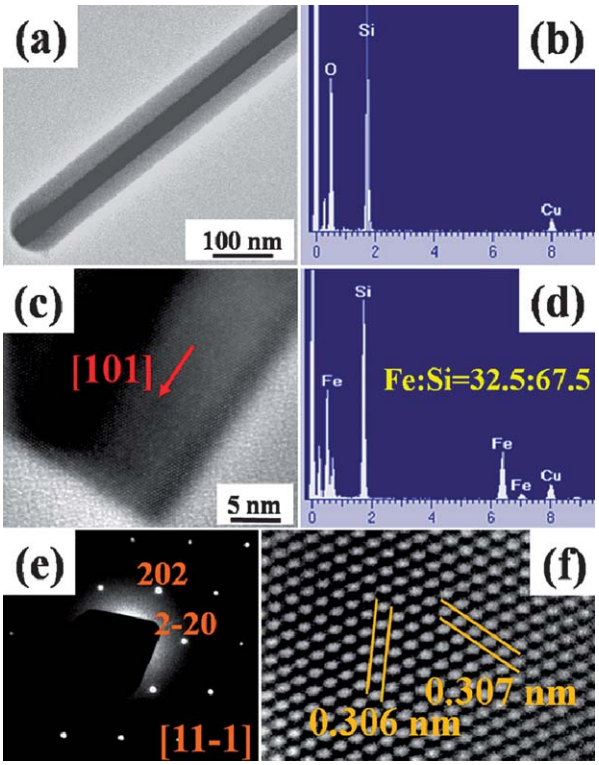

Fig. 2 Representative TEM analyses of the core–shell β-$FeSi_2$ nanowires: (a) a low-magnification image of a nanowire with a core–shell structure, (b) the EDS spectrum shows that the shell layer is composed of Si and O, (c) a high-magnification image of a β-$FeSi_2$ nanowire with the silicon oxide shell layer removed, (d) the EDS analysis shows the chemical composition of Fe : Si is close to 1 : 2, (e) the SAED pattern indicating that the β-$FeSi_2$ is single-crystalline, and (f) a HRTEM image confirming that the nanowire is β-$FeSi_2$.

obtained from a representative nanowire, which can be indexed to an orthorhombic β-$FeSi_2$ structure (a = 0.9863 nm, b = 0.7791 nm and c = 0.7833 nm) and demonstrates that the nanowire growth is along the [101] direction. The corresponding high-resolution TEM (HRTEM) image is shown in Fig. 2(f) and clearly presents the single-crystalline structure of the nanowire, without linear or planar defects. The two d-spacings of 0.306 nm and 0.307 nm were identified to correspond to β-$FeSi_2$ (2-20) and (202) planes, respectively.

The reactions of the evaporated $FeCl_3$ precursor vapor with the silicon substrates at the hot zone of the furnace to form the β-$FeSi_2$ nanowires may follow two reaction pathways

$$4\ FeCl_{3(g)} + 11\ Si_{(s)} \leftrightarrow 4\ \beta\text{-}FeSi_{2(s)} + 3\ SiCl_{4(g)}$$

$$2\ FeCl_{3(g)} + 4\ SiCl_{4(g)} \leftrightarrow 2\ \beta\text{-}FeSi_{2(s)} + 11\ Cl_{2(g)}$$

In previous works, several sets of experimental evidence also indicated that silicide nanowires were fabricated by a vapor–solid mechanism.[26,27] In our cases, no catalyst particles were found on the tip of the nanowires, suggesting that our nanowire growth was not *via* the typical vapor–liquid–solid growth mechanism.[28]

The growth processes of the iron silicide nanowires included two steps. First, the silicide particles were formed on the substrates. Second, self-catalyzed nanowires were grown from the silicide particles.[29] Both the vapor flux of the precursors and the reaction temperature were found to be critically important in our growth system (see ESI S1 and S2).† When the Si substrates containing vapor precursors were positioned in region B of the furnace, only sheet structures were found. On the other hand, high yield β-$FeSi_2$ nanowires could be obtained when the optimum synthesis conditions for nanowire growth were performed in region C. Region D was far away from the precursors and the vapor flux was expected to be the lowest. Lower growth density of the core–shell β-$FeSi_2$ nanowires were obtained compared with products grown in region C. The detailed characterization for structures and compositions of β-$FeSi_2$ nanowire formed in region D is described in ESI S3.†

Fig. 3(a) shows the room-temperature PL spectrum of the β-$FeSi_2$ nanowires excited by a 405 nm laser and exhibits an emission peak at a wavelength of 1.54 μm. β-$FeSi_2$ is known as a semiconducting material with a band gap near 0.8 eV, which is

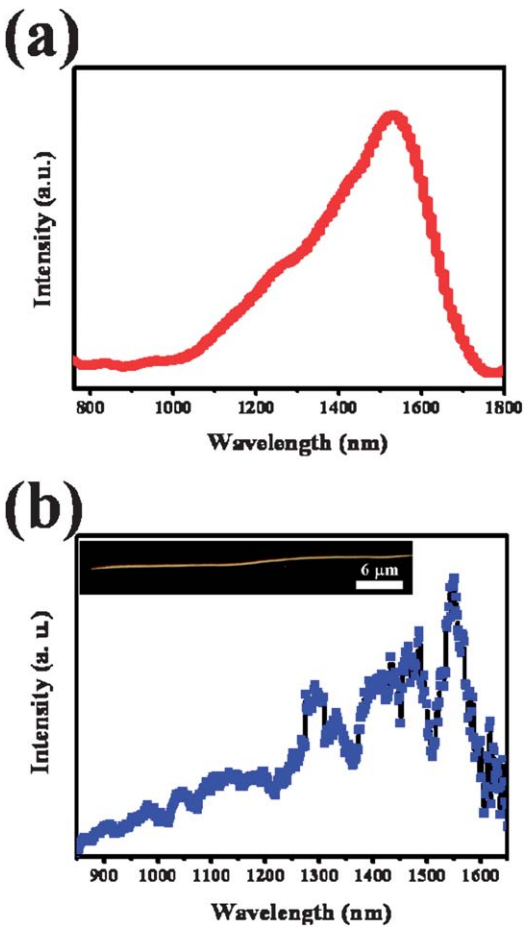

Fig. 3 (a) A room temperature photoluminescence spectrum of the β-$FeSi_2$ nanowires excited by a 405 nm laser. An emission peak at a wavelength of 1.54 μm can be observed. (b) A room temperature NIR PL spectrum obtained from the single-stem β-$FeSi_2$ nanowire. The spectrum also shows the emission peak at the wavelength 1.54 μm. Inset: a dark-field image of the single β-$FeSi_2$ nanowire obtained from the optical microscope.

suitable for optical communication due to its band gap being near the absorption minimum of fibers. For the optical applications of β-$FeSi_2$ nanostructures, several factors were found to be important for luminescence enhancement. For example, low temperature measurements were normally carried out to avoid thermal fluctuations. A previous report indicated that for the enhancement of PL efficiency, high quality β-$FeSi_2$ with suitable strain at the interface between β-$FeSi_2$ and Si substrates is needed.[20] Furthermore, suitable strain will transform β-$FeSi_2$ from indirect-gap to direct-gap characteristics,[30,31] suggesting higher luminescence efficiency can be obtained. A defect-free single-crystalline structure also plays a key role in the luminescence enhancement of β-$FeSi_2$.[32] The emission intensity was proportional to the annealing time,[33] which suggested that crystallinity dominates the luminescence efficiency. In addition, in order to eliminate interface defects between β-$FeSi_2$ and Si, the thermal annealing process is very important. Maeda[16] has reported the intrinsic luminescence of β-$FeSi_2$ at 0.805 eV (1.55 μm), and others at 0.839 eV (1.48 μm) and 0.754 eV (1.65 μm) originated from extrinsic luminescence. Luminescence efficiency resulting from exciton confinement in β-$FeSi_2$ is also discussed. On the other hand, the present study found that single-crystalline β-$FeSi_2$ nanowires with band-edge luminescence can be facilely synthesized *via* a chemical reaction method in one step without the complications of inducing the interface strain as well as annealing.

Photoluminescence and electroluminescence properties for embedding β-$FeSi_2$ in Si were previously investigated.[20] Suitable strain in the as-synthesized β-$FeSi_2$ was found to be a critical issue for the PL properties of β-$FeSi_2$. To further clarify the PL property of the β-$FeSi_2$ nanowire, the PL behavior in NIR for a single β-$FeSi_2$ nanowire was also investigated. Fig. 3(b) shows the room-temperature NIR PL spectrum of a single-stem β-$FeSi_2$ nanowire. The length of the single β-$FeSi_2$ nanowire is about 40 μm. A dark-field optical microscope image is shown in the inset. The individual nanowire shows emission in the visible region, which mostly comes from scattering light in ambient air. In the single nanowire NIR PL spectrum, the room-temperature PL peak at a wavelength of 1.54 μm can be observed. The band-edge luminescence of the β-$FeSi_2$ nanowire is correlated to the single-crystalline structure, as seen in the TEM images shown in Fig. 2. Compared with the spectrum shown in Fig. 3(a), the PL spectrum of the single β-$FeSi_2$ nanowire shows some shoulder peaks. These peaks are suggested to be due to the defects or dangling bonds present on the nanowire surface, which will result in the variation of the nanowire surface states.

The electrical properties of the single-stem β-$FeSi_2$ nanowire were measured by the two-terminal *I–V* method. The current output of the β-$FeSi_2$ nanowires is shown in Fig. 4(a). The diameter of the nanowire is one of the significant factors that affect resistivity. To find the electrical transport properties, measurements were conducted for nanowires of various sizes. The current density was found to increase with decreasing nanowire diameter. The estimated resistivity as a function of nanowire diameter and the linear fitting characteristics of the plot are shown in Fig. 4(b). It shows little or no contact resistance in our nanodevices. The increase in conductivity with decreasing diameter is likely to be due to more enhanced surface conductivity.[34] Recent research on the electrical properties of β-$FeSi_2$

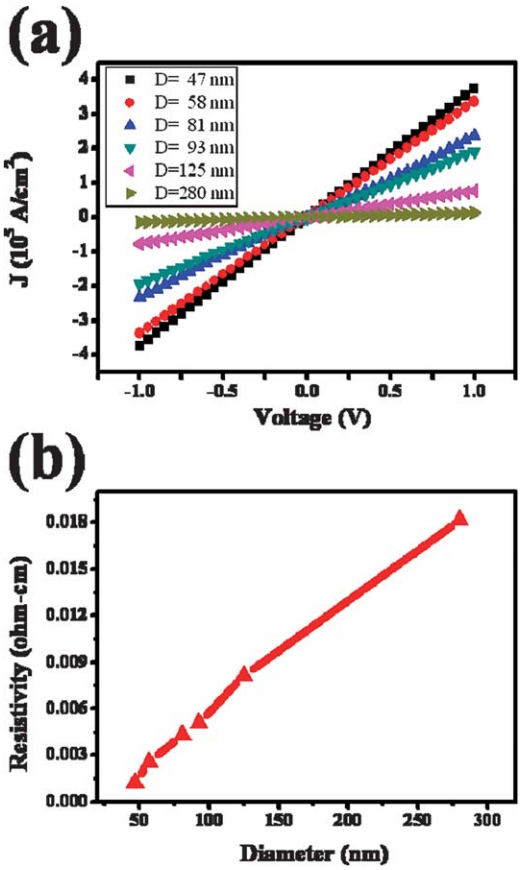

Fig. 4 (a) Electrical transport measurements of β-$FeSi_2$ nanowires with various sizes. Inset: a SEM image of the single-stem nanowire with Pt electrodes. (b) The resistivities of the various sizes of β-$FeSi_2$ nanowires. The resistivity of a nanowire decreases with reducing nanowire diameter.

thin films showed higher resistivity compared to the nanowires reported herein. In our previous work, Lu *et al.*[35] estimated the resistivity of β-$FeSi_2$ thin films as 0.022 Ω cm. The measured resistivity of a 47 nm β-$FeSi_2$ nanowire is 0.00123 Ω cm, which is over one order of magnitude lower than that of thin films.

Fig. 5(a) shows the room-temperature VSM hysteresis loop curves of the as-grown β-$FeSi_2$ nanowires with applied magnetic fields parallel and perpendicular to the substrates. (sample preparation, see ESI S4).† The hysteresis loop for the case of the applied magnetic field parallel to the substrates has a relatively hard magnetization axis and high remanence (residual magnetization) with a coercive field of 118 Oe. On the other hand, the hysteresis loop for the case of the applied magnetic field perpendicular to the substrates has an easy magnetization axis and low remanence (residual magnetization) with a coercive field of about 90 Oe. The ferromagnetic behavior at room temperature can be observed in as-synthesized β-$FeSi_2$ nanowires. In contrast, in the β-$FeSi_2$ thin film case, ferromagnetism was found only at temperatures below 100 K.[36] The ferromagnetism observed in the β-$FeSi_2$ nanowires is attributed to the reduced coordination of the surface Fe atoms in the β-$FeSi_2$ nanowires.[37] These non-stoichiometric regions may act as a ferromagnetic surface layer on the nanowires, in which the surface-to-volume ratio is high while the system size is reduced to the nanoscale in one or more dimensions. The high remanence and coercive field in nanowires

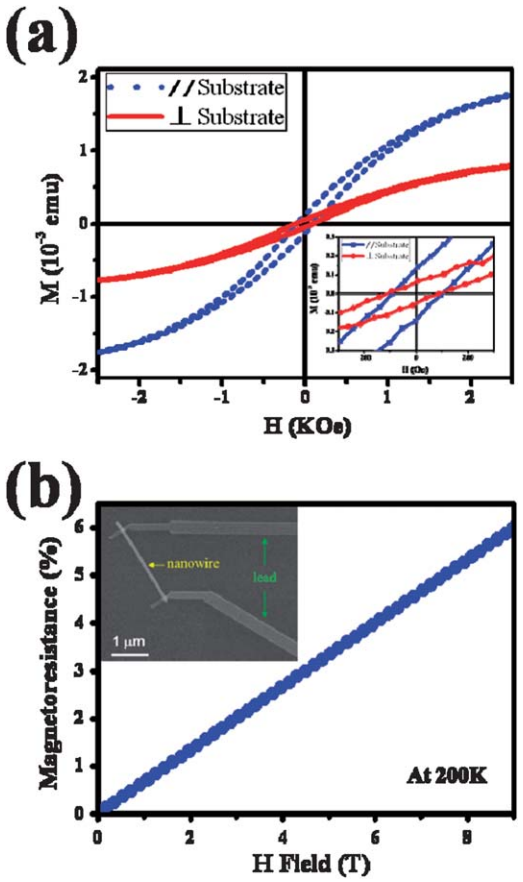

Fig. 5 (a) Hysteresis loop curves of the β-$FeSi_2$ nanowires at room temperature with magnetic fields applied parallel and perpendicular to the substrates. The inset shows the loops on an enlarged scale. (b) Magnetotransport measurements of an individual single-stem β-$FeSi_2$ nanowire with the applied transverse field (up to 9 T) at 200 K. A magnetoresistance variation of 6% can be observed. Inset: A SEM image of the β-$FeSi_2$ nanodevice fabricated with standard e-beam lithography processes.

are attributed to the shape anisotropy effect, which forces the magnetic moments to mostly align along the axis of the nanowires.[38]

Recently, strong hysteretic magnetoresistance (MR) features of nominally nonferromagnetic silicide films and nanowires were reported. The MR effects were found to be quenched at temperatures of a few Kelvins.[39] The MR of an individual single-stem β-$FeSi_2$ nanowire was measured as a function of the transverse applied magnetic field. The MR is defined as $MR = [R(H) - R(0)]/R(0)$, where $R(H)$ and $R(0)$ are the resistance at the applied transverse field (up to 9 T) and zero field, respectively. The typical nanodevice is shown in SEM image in the inset of Fig. 5(b) (for nanodevice fabrication, see ESI S5).† For the observation, the intrinsic positive MR is shown in Fig. 5 (b). Similar magnetic behavior was reported in semiconducting $Fe_{1-x}Co_xSi$ systems. Jin and coworkers[40] indicated that $Fe_{1-x}Co_xSi$ nanowires showed large MRs of 4.9 and 8.7% at an applied field of 9 T. The temperature was cooled down to as low as 2 K. However, they also found a negative MR of 6 and 9.7% at 9 T (temperature: 5 K) in magnetic CrO_2 nanorods.[41] As mentioned above, the MR effect can be observed by cooling the samples to a few Kelvins. As shown in our data, a maximum MR of 6% can be observed at the highest magnetic field of 9 T at 200 K. In general, for semiconductor materials, resistance variation under an applied magnetic field can be attributed to several factors, such as material shape (shape effect), carrier density and carrier mobility. MR effects in silicide nanostructures can be accounted for by the interaction of conducting electrons with localized dangling bonds spins, and this interaction has dramatic consequences for transport when the system size is reduced to the nanoscale.[39] The room temperature ferromagnetic behavior and the large MR effect seen in the nanodevice indicate that magnetic semiconducting β-$FeSi_2$ can be employed in versatile applications in the field of spintronics, such as spin injection electrodes in tunneling magnetoresistance (TMR) devices.

Conclusions

In summary, free-standing β-$FeSi_2$ nanowires with a high aspect ratio have been synthesized *via* a spontaneous chemical vapor transport growth method in one step. The resulting self-catalyzed β-$FeSi_2$ nanowires exhibit room temperature photoluminescence properties at a wavelength of 1.54 μm, which is attributed to the single-crystalline structure. A room temperature emission peak at 1.54 μm was also observed in the NIR PL spectra for individual β-$FeSi_2$ nanowires. The resistivity of the nanowires was found to decrease with reducing nanowire diameter due to the enhanced surface conductivity in smaller nanowires. The discoveries of room temperature ferromagnetic behavior and the large MR performance of 6% at 200 K indicate that β-$FeSi_2$ nanowires have great potential for applications in spintronic nanodevices. Based on the room temperature photoluminescence and ferromagnetism, as well as favorable electrical transport and magnetotransport properties, β-$FeSi_2$ is potentially applicable in Si-based optoelectronic and spintronic devices.

Acknowledgements

The research was supported by the Republic of China National Science Council grants no. NSC 96-2221-E-007-169-MY3 and NSC 97-2120-M-007-003.

Notes and references

1 Z. Zhong, D. Wang, Y. Cui, M. W. Bockrath and C. M. Lieber, *Science*, 2003, **302**, 1377.
2 L. J. Chen, *J. Mater. Chem.*, 2007, **17**, 4639.
3 K. C. Chen, W. W. Wu, C. N. Liao, L. J. Chen and K. N. Tu, *Science*, 2008, **321**, 1066.
4 C. H. Lai, K. W. Huang, J. H. Cheng, C. Y. Lee, B. J. Hwang and L. J. Chen, *J. Mater. Chem.*, 2010, **20**, 6638.
5 C. H. Lai, K. W. Huang, J. H. Cheng, C. Y. Lee, W. F. Lee, C. T. Huang, B. J. Hwang and L. J. Chen, *J. Mater. Chem.*, 2009, **19**, 7277.
6 W. Lu and C. M. Lieber, *Nat. Mater.*, 2007, **6**, 841.
7 A. I. Hochbaum, R. Chen, R. D. Delgado, W. Liang, E. C. Garnett, M. Najarian, A. Majumdar and P. Yang, *Nature*, 2008, **451**, 163.
8 Y. Wang, K.-K. Lew, T.-T. Ho, L. Pan, S. W. Novak, E. C. Dickey, J. M. Redwing and T. S. Mayer, *Nano Lett.*, 2005, **5**, 2139.
9 E. C. Garnett, W. Liang and P. Yang, *Adv. Mater.*, 2007, **19**, 2946.
10 B. Tian, X. Zheng, T. J. Kempa, Y. Fang, N. Yu, G. Yu, J. Huang and C. M. Lieber, *Nature*, 2007, **449**, 885.
11 Y. Wu, R. Fan and P. Yang, *Nano Lett.*, 2002, **2**, 83.

12 S. H. Oh, K. v. Benthem, S. I. Molina, A. Y. Borisevich, W. Luo, P. Werner, N. D. Zakharov, D. Kumar, S. T. Pantelides and S. J. Pennycook, *Nano Lett.*, 2008, **8**, 1016.
13 B.-S. Kim, T.-W. Koo, J.-H. Lee, D. S. Kim, Y. C. Jung, S. W. Hwang, B. L. Choi, E. K. Lee, J. M. Kim and D. Whang, *Nano Lett.*, 2009, **9**, 864.
14 C. Dais, G. Mussler, H. Sigg, T. Fromherz, V. Auzelyte, H. H. Solak and D. Grützmacher, *Europhys. Lett.*, 2008, **84**, 67017.
15 D. Leong, M. Harry, K. J. Reeson and K. P. Homewood, *Nature*, 1997, **387**, 686.
16 Y. Maeda, *Appl. Surf. Sci.*, 2008, **254**, 6242.
17 A. Imai, S. Kunimatsu, K. Akiyama, Y. Terai and Y. Maeda, *Thin Solid Films*, 2007, **515**, 8162.
18 Y. Y. Maeda, K. P. Homewood, T. Suemasu, T. Sadoh, H. Udono and K. Yamaguchi, *Thin Solid Films*, 2004, **461**, 1.
19 S. Chu, T. Hirohada, M. Kuwabara, H. Kan and T. Hiruma, *Jpn. J. Appl. Phys.*, 2004, **43**, 127.
20 T. Suemasu, Y. Negishi, K. Takakura and F. Hasegawa, *Appl. Phys. Lett.*, 2001, **79**, 1804.
21 S. Liang, R. Islam, D. J. Smith and P. A. Bennett, *J. Cryst. Growth*, 2006, **295**, 166.
22 K. Yamamoto, H. Kohno, S. Takeda and S. Ichikawa, *Appl. Phys. Lett.*, 2006, **89**, 083107.
23 N. Manyala, Y. Sidis, J. F. DiTusa, G. Aeppli, D. P. Young and Z. Fisk, *Nature*, 2000, **404**, 581.
24 N. Manyala, Y. Sidis, J. F. Ditusa, G. Aeppli, D. P. Young and Z. Fisk, *Nat. Mater.*, 2004, **3**, 255.
25 P. Lengsfeld, S. Brehme, G. Ehlers, H. Lange, N. Stüsser, Y. Tomm and W. Fuhs, *Phys. Rev. B: Condens. Matter*, 1998, **58**, 16154.
26 C. M. Chang, Y. C. Chang, Y. A. Chung, C. Y. Lee and L. J. Chen, *J. Phys. Chem. C*, 2009, **113**, 17720.
27 B. S. Guiton, Q. Gu, A. L. Prieto, M. S. Gudiksen and H. Park, *J. Am. Chem. Soc.*, 2002, **127**, 498.
28 A. M. Morales and C. M. Lieber, *Science*, 1998, **279**, 208.
29 C. I. Tsai, P. H. Yeh, C. Y. Wang, H. W. Wu, U. S. Chen, M. Y. Lu, W. W. Wu, L. J. Chen and Z. L. Wang, *Cryst. Growth Des.*, 2009, **9**, 4514.
30 S. J. Clark, H. M. Al-Allak, S. Brand and R. A. Abram, *Phys. Rev. B: Condens. Matter*, 1998, **58**, 10389.
31 D. B. Migas and L. Miglio, *Phys. Rev. B: Condens. Matter*, 2000, **62**, 11063.
32 L. J. Chen, S. Y. Chen and H. C. Chen, *Thin Solid Films*, 2007, **515**, 8140.
33 Y. Maeda, Y. Terai, M. Itakura and N. Kuwano, *Thin Solid Films*, 2004, **461**, 160.
34 D. K. Lim, O. Kubo, Y. Shingaya, T. Nakayama, Y. H. Kim, J. Y. Lee, M. Aono, H. Lee, D. Lee and S. Kim, *Appl. Phys. Lett.*, 2008, **92**, 203114.
35 H. T. Lu, Y. L. Chueh, L. J. Chou and L. J. Chen, *Appl. Surf. Sci.*, 2003, **212**, 204.
36 O. Valassiades, C. A. Dimitriadis and J. H. Werner, *J. Appl. Phys.*, 1991, **70**, 890.
37 K. Seo, K. S. K. Varadwaj, P. Mohanty, S. Lee, Y. Jo, M.-H. Jung, J. Kim and B. Kim, *Nano Lett.*, 2007, **7**, 1240.
38 Y. L. Chueh, L. J. Chou, J. Song and Z. L. Wang, *Nanotechnology*, 2007, **18**, 145604.
39 T. Kim, B. Naser, R. V. Chamberlin, M. V. Schilfgaarde, P. A. Bennett and J. P. Bird, *Phys. Rev. B: Condens. Matter Mater. Phys.*, 2007, **76**, 184404.
40 A. L. Schmitt, J. M. Higgins and S. Jin, *Nano Lett.*, 2008, **8**, 810.
41 Y. Song, A. L. Schmitt and S. Jin, *Nano Lett.*, 2008, **8**, 2356.